Bull. Mater. Sci., Vol. 36, No. 5, October 2013, pp. 859–868. © Indian Academy of Sciences.

Structural and mechanical behaviour of 5% Al_2O_3-reinforced Fe metal matrix composites (MMCs) produced by powder metallurgy (P/M) route

PALLAV GUPTA, DEVENDRA KUMAR*, OM PARKASH and A K JHA†

Department of Ceramic Engineering, †Department of Mechanical Engineering, Indian Institute of Technology (Banaras Hindu University), Varanasi 221 005, India

MS received 13 February 2012; revised 27 May 2012

Abstract. **The aim of this paper is to investigate the effect of sintering temperature and time on the properties of Fe–Al_2O_3 composite (5 wt% Al_2O_3; 95 wt% Fe) prepared by powder metallurgy process. X-ray diffraction, microstructure, density, hardness and compressive strength of prepared samples have been investigated. XRD studies show the presence of Fe and Al_2O_3 along with iron aluminate phase. Iron aluminate is formed as a result of reactive sintering between iron and alumina particles. Microstructural examination of the specimen showed a dense structure with nanosize dispersion of the reinforcement of ceramic phase. Density as well as hardness of specimens depend on the formation of iron aluminate phase, which in turn depends on sintering temperature and time.**

Keywords. **Metal matrix composite (MMC); XRD; SEM; density; hardness; compressive strength.**

1. Introduction

Metal matrix composites (MMCs) have gained a considerable interest in the last three decades. The driving force has been the fact that addition of ceramic reinforcement in the metallic matrix can improve specific strength, stiffness, wear, fatigue and creep properties compared to conventional engineering materials (Tjong and Ma 2000; Rabiei *et al* 2008). MMCs are widely used in several industrial areas such as aerospace, automotive and electronics (Aldas and Mat 2005; Mehdi *et al* 2009). It has been observed that properties of MMCs are greatly influenced by the nature of reinforcement and its distribution in the metal matrix (Roy *et al* 2006). Properties of the composites are also influenced by the chemical nature of components, morphology of particles, their distribution and interface reactions (Reddy *et al* 2008). Particle size, however, is an important factor which is directly related to the strength of the composites (Wei 2001; Chen and Wang 2002). There has been significant advancements in the processing techniques to control the microstructure and resulting mechanical properties of MMCs (Shen and Chawla 2001). The processing methods utilized to manufacture MMCs can be grouped according to the temperature of metallic matrix during processing (Pagounis *et al* 1996). MMCs, in general, are fabricated mostly using powder metallurgy (P/M) and stir casting techniques (Fligier *et al* 2008). It is the economical aspect which will decide the processing route. In order to lower the cost and to improve the properties, solid state technique, i.e. powder metallurgy route, is of significant importance (Rosso 2006). The extended advantage of using P/M technique is that it makes use of lower temperature as compared to other processing methods and there is less interaction between the matrix and the reinforcement (Torralba *et al* 2003). P/M technique gives more homogenous distribution of particles in the metal matrix with or without interaction between the matrix and reinforcement phase (Chua *et al* 1999). Lot of work has been done using aluminum as the matrix material but there are very few reports using iron as metal matrix (Fedorchenko and Ivanova 1969; Pagounis *et al* 1996). The aim of the present paper is to investigate the effect of sintering temperature and time on densification, phase, microstructure, hardness and compressive strength of Fe–Al_2O_3 composite (5 wt% Al_2O_3; 95 wt% Fe) prepared by powder metallurgy process. Fe–Al_2O_3 composites find applications in heavy duty components like railway wagon wheels, etc where pure iron cannot give superior structural and mechanical properties (Miracle 2005).

2. Experimental

2.1 *Preparation*

Iron powder having 99·5% purity and particle size in the range of 250–300 mesh and active aluminum oxide having particle size of 70–230 mesh are used as starting materials. Composite selected for investigation contains 95 wt% Fe and 5 wt% Al_2O_3. Mixed powder was dry ball milled with the powder to ball ratio of 1:2 using zirconia balls as the grinding and mixing media (Karak *et al* 2012). Initially the powder of electrolytic iron (Fe) and aluminum oxide (Al_2O_3) was milled in the ball mill for a period of 1 h. Thereafter, 1%

*Author for correspondence (devendra.cer@iitbhu.ac.in)

glycerine and 1% dextrin were added to the above mixture and the whole mixture was milled for a period of 1 h again. Mixed powders were compacted using a hydraulic press under a constant load of 7 tons in a die of 13 mm diameter. Green compacts were sintered in an argon atmosphere in the temperature range of 900–1100 °C for 1–3 h. After sintering, the compacts were machined on gap or extension type lathe machine using a four jaw independent chuck. Thereafter, surface of the specimens was polished. A nomenclature, e.g. 5AFe900(1), is given to each specimen. Here A denotes the aluminum oxide, Fe denotes iron, 900 denotes the sintering temperature and 1 denotes time of sintering in h. Nine specimens were prepared using different time and temperatures of sintering.

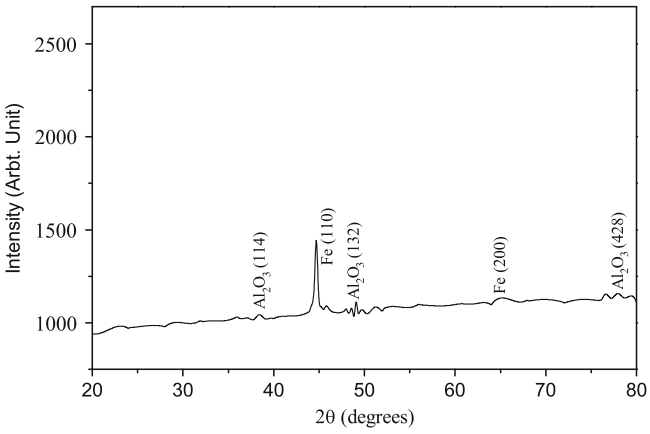

Figure 1. XRD pattern of ball milled powder.

2.2 *Measurements*

Phase determination was done by powder X-ray diffraction (XRD) using Rigaku Desktop Miniflex II X-ray diffractometer employing CuKα radiation and Ni-filter. Microstructure was studied using Inspect S-50, FP 2017/12 scanning electron microscope. Cylindrical samples of 12 mm diameter and

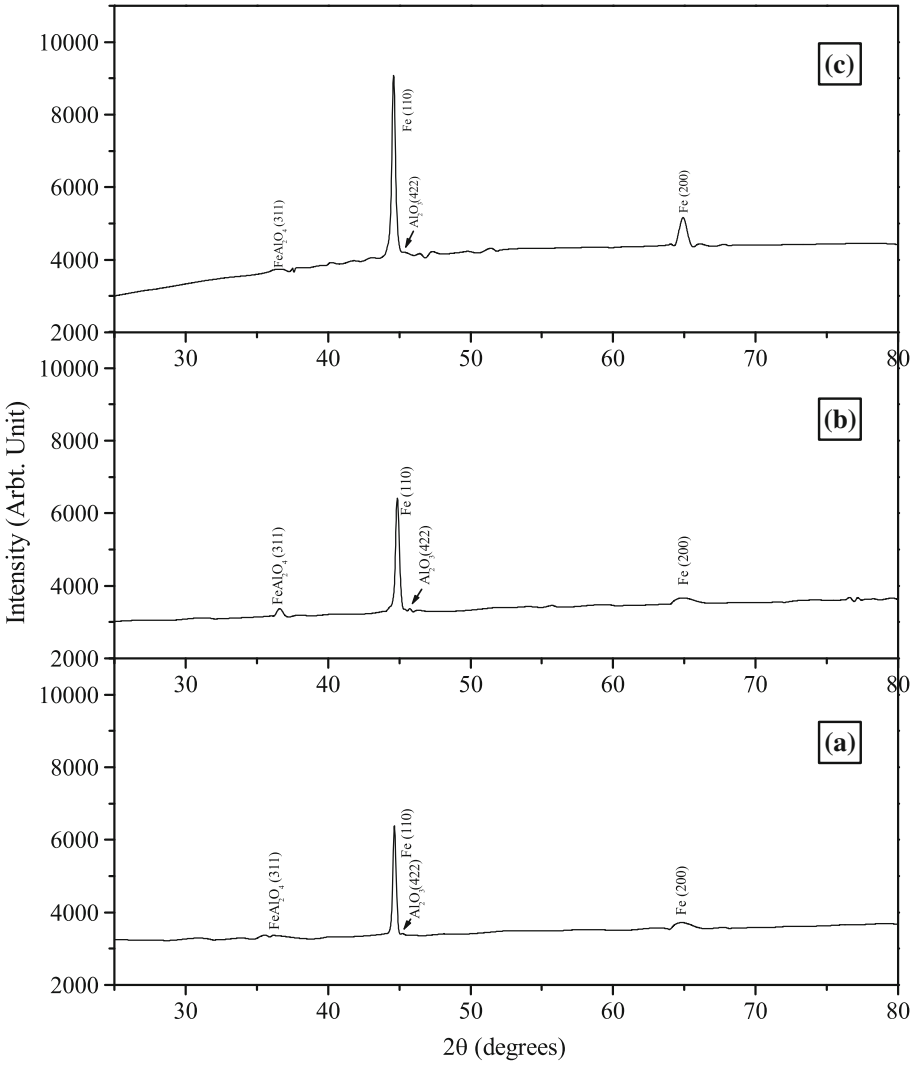

Figure 2. XRD patterns of specimens: (**a**) 5AFe900(1), (**b**) 5AFe1000(1) and (**c**) 5AFe1100(1).

2 mm thickness were used for SEM studies. The samples were polished using various grades of the emery paper (1/0, 2/0, 3/0 and 4/0) and then finally on the diamond polish. Polished samples were etched using concentrated hydrochloric acid for 20 s.

Density was determined from mass and dimensions. Hardness was measured on a Rockwell Hardness Tester using 1/8″ H scale steel ball indenter having a major loading capacity of 60 kg. The reading of H type indenter can be read on the red scale present on the dial gauge of the instrument. Compressive strength was determined using a 5 Ton Instron Universal Testing machine (UTM).

3. Results and discussion

3.1 *X-ray diffraction*

X-ray diffraction pattern of ball milled powder has been shown in figure 1. Diffraction peaks present in the specimen were matched with the XRD-JCPDS files of different compounds. It was found that only iron and alumina were present in the ball milled powder and there was no reaction between the constituent materials during ball milling.

X-ray diffraction patterns of specimens sintered at different temperatures for 1 h are shown in figure 2. Diffraction peaks of specimen 5AFe900(1), 5AFe1000(1) and 5AFe1100(1) were matched with the XRD-JCPDS files of different compounds of constituent elements. It was found that a small amount of $FeAl_2O_4$ as a minor phase and Fe as a major phase are present in the composite specimens (Konopka and Ozieblo 2001). Unreacted Al_2O_3 may also be present in the specimen. This shows that a reaction between iron and alumina takes place leading to the formation of iron aluminate ($FeAl_2O_4$) during the sintering process. Thus, in this Fe–Al_2O_3 composite system sintering is reactive sintering and $FeAl_2O_4$ is dispersed in Fe matrix.

X-ray diffraction pattern of the specimens sintered for 2 h are shown in figure 3. Again, the matching of specimen

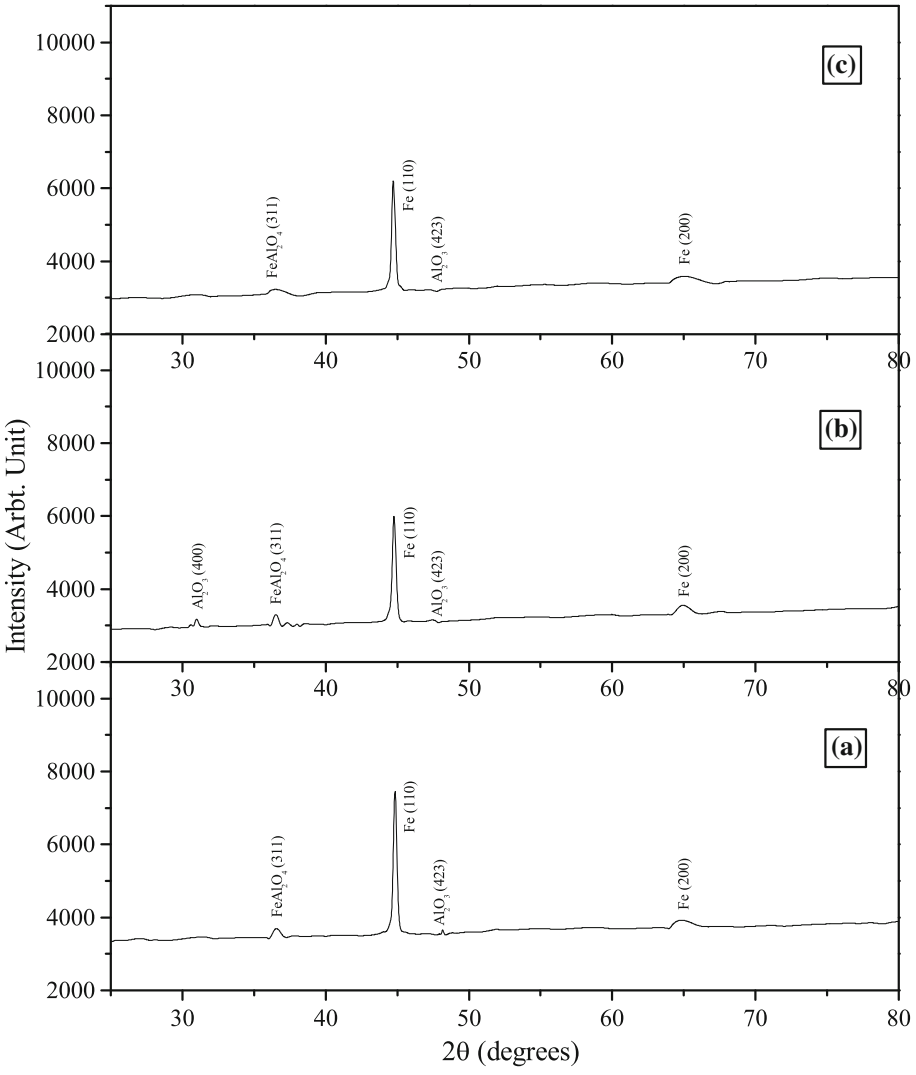

Figure 3. XRD patterns of specimens: (**a**) 5AFe900(2), (**b**) 5AFe1000(2) and (**c**) 5AFe1100(2).

5AFe900(2), 5AFe1000(2) and 5AFe1100(2) was done in a similar fashion as for specimen sintered for 1 h. From this matching, it was found that in specimen 5AFe900(2), iron aluminate phase and iron phase are present. Specimen 5AFe1000(2) shows presence of Al_2O_3, $FeAl_2O_4$ and major amount of Fe phases in the composite. This shows that similar to the specimens sintered for 1 h, a reaction between iron and alumina takes place leading to the formation of iron aluminate ($FeAl_2O_4$) during sintering process.

X-ray diffraction pattern of specimens sintered for 3 h is shown in figure 4. Specimen 5AFe1000(3) shows formation of $FeAl_2O_4$ along with major amount of Fe. Specimen 5AFe1100(3) shows presence of $FeAl_2O_4$ along with major amount of Fe. The number of peaks present in 5AFe1000(3) and 5AFe1100(3) are same indicating that similar to the specimens sintered for 1 and 2 h, a reaction between iron and alumina takes place leading to the formation of iron aluminate ($FeAl_2O_4$) during sintering process. Thus, also in this Fe–Al_2O_3 composite system sintering is reactive sintering and $FeAl_2O_4$ is dispersed in Fe matrix.

3.2 *Microstructure*

To investigate the sintering development of phase and microstructure, micrographs of all the specimens were recorded at different magnifications ranging from 2000X to 15000X using SEM. In this paper, we are reporting the microstructures of specimens 5AFe900(3), 5AFe1000(3), 5AFe1100(1) and 5AFe1100(3).

Figure 5 shows SEM micrographs of specimen 5AFe900(3), sintered at 900 °C for 3 h, at 2000X, 5000X and 15000X, respectively. The micrograph at 2000X magnification reveals the formation of highly dense Fe–Al_2O_3 composite. The dense phase has negligible amount of porosity. Figure 5(b) shows grains with the presence of small uneven shaped pores. It also shows three types of grains, white ones are of aluminum oxide, black are of iron and greyish are of iron aluminate, respectively. Figure 5(c) shows micrograph at 15000X magnification, which shows formation of nanosize particles of iron aluminate phase. The size of the particle lies in the range of 130–265 nm.

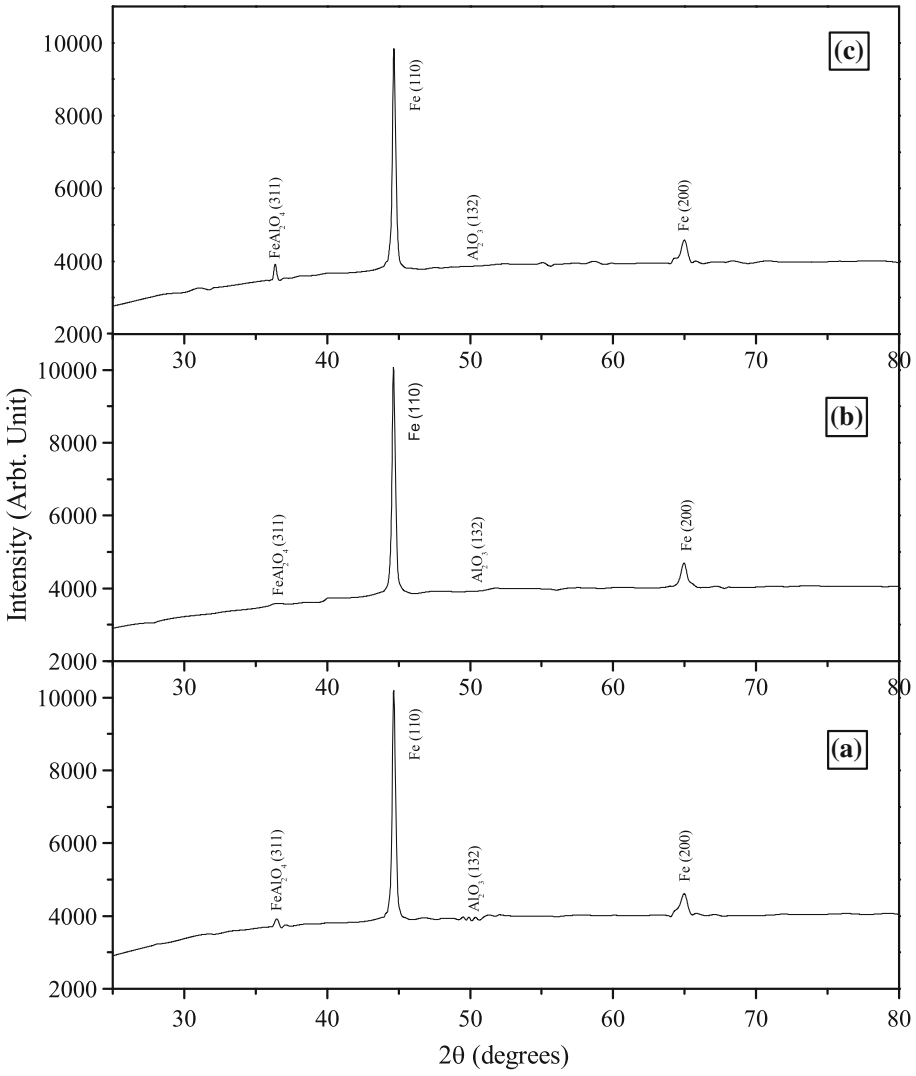

Figure 4. XRD pattern of specimens: (**a**) 5AFe900(3), (**b**) 5AFe1000(3) and (**c**) 5AFe1100(3).

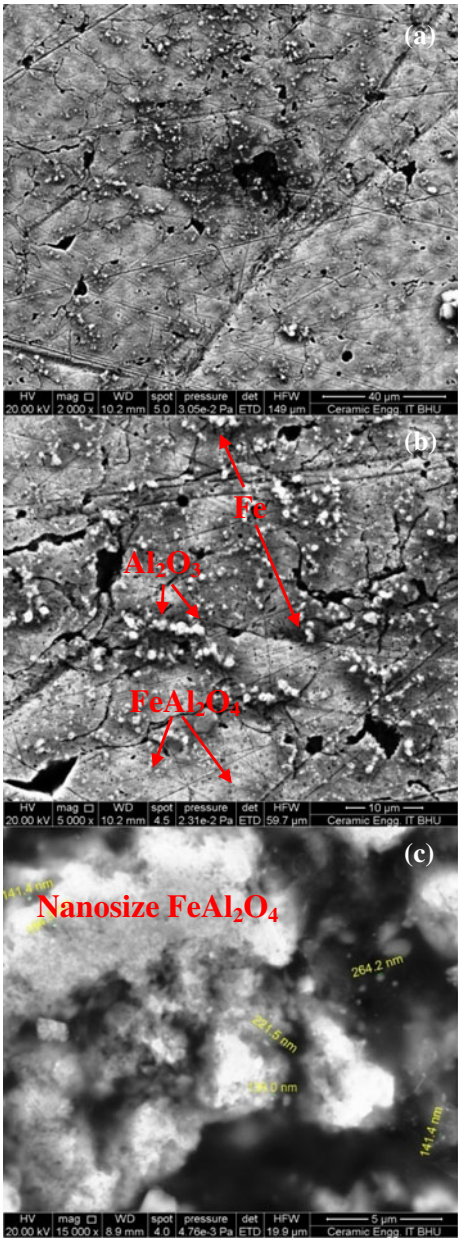

Figure 5. SEM micrographs of 5AFe900(3): (**a**) 2000X, (**b**) 5000X and (**c**) 15000X magnifications.

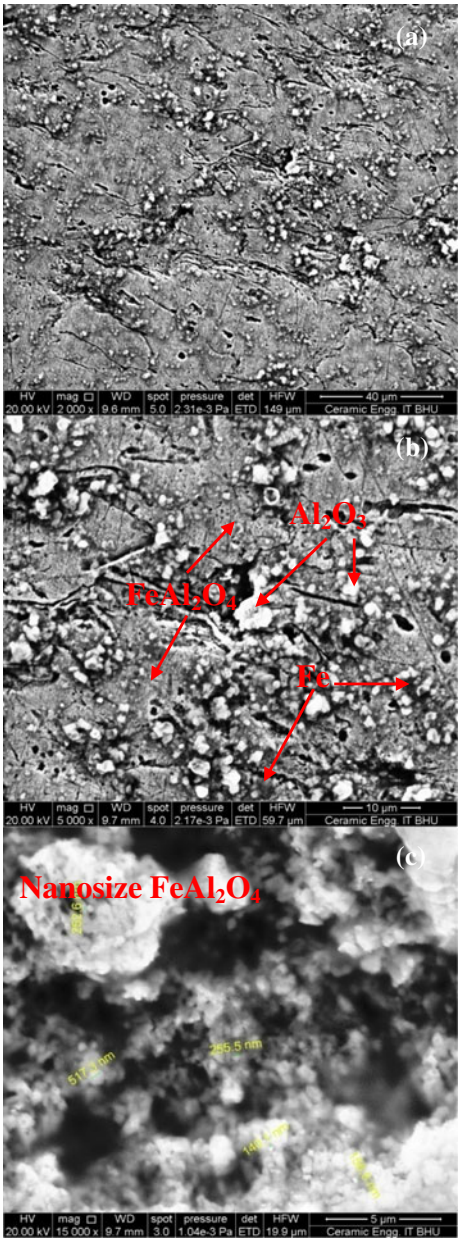

Figure 6. SEM micrographs of 5AFe1000(3): (**a**) 2000X, (**b**) 5000X and (**c**) 15000X magnifications.

SEM micrograph of specimen 5AFe1000(3), sintered at 1000 °C for 3 h, at 2000X, 5000X and 15000X are shown in figure 6. The microstructure shows dense phase formation of Fe–Al_2O_3 composite (figure 6a). Negligible amount of porosity is present in the specimen. The various particles, i.e. of iron, alumina and iron aluminate, present in the microstructure have been marked on the micrographs. The microstructure at 5000X as indicated in figure 6(b) shows bigger alumina particles of size 1–4 μm and some smaller grains are of Al_2O_3. The remaining some smaller and some larger grains are of iron aluminate. The iron aluminate formed here is due to reactive sintering between iron and alumina particles. Figure 6(c) shows same iron aluminate phase at nano-size level in the range of 150–500 nm.

SEM micrograph of specimen 5AFe1100(3), sintered at 1100 °C for 3 h, at 2000X, 5000X and 15000X are shown in figure 7. Figure 7(a) shows highly dense phase composite along with uniform size grains. The microstructure shows negligible amount of porosity that is present. Figure 7(b) shows grains of iron aluminate, alumina and iron. It also shows micron sized particles of alumina and iron aluminate, respectively. Figure 7(c) shows nano size formation of particles of alumina and iron aluminate, respectively. The specimen 5AFe1100(3) is more dense in comparison to specimen 5AFe1000(3) and 5AFe900(3).

To show the effect of sintering time, SEM micrographs of specimen 5AFe1100(1), sintered at 1100 °C for 1 h at 2000X, 5000X and 15000X are also shown in figure 8.

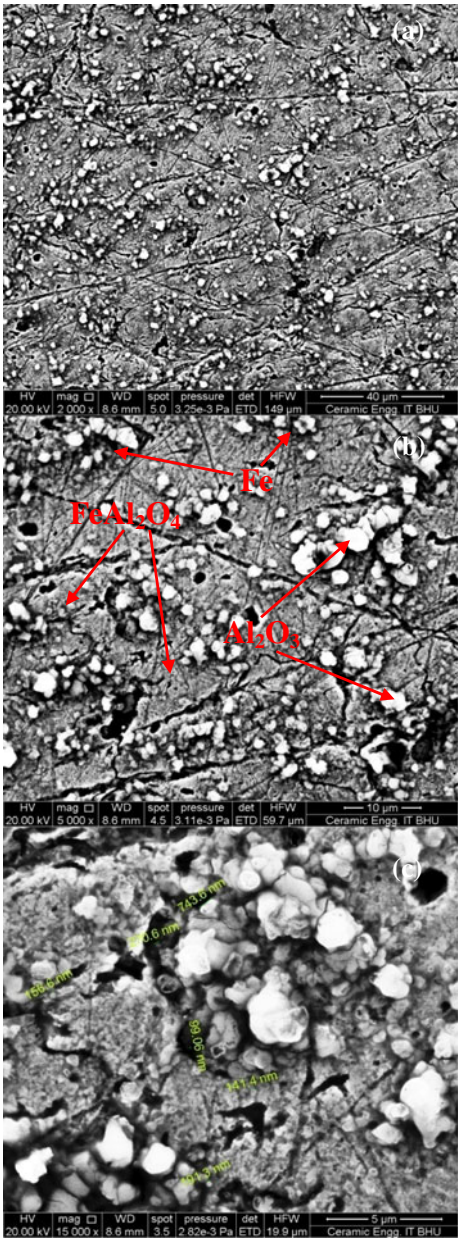

Figure 7. SEM micrographs of 5AFe1100(3): (**a**) 2000X, (**b**) 5000X and (**c**) 15000X magnifications.

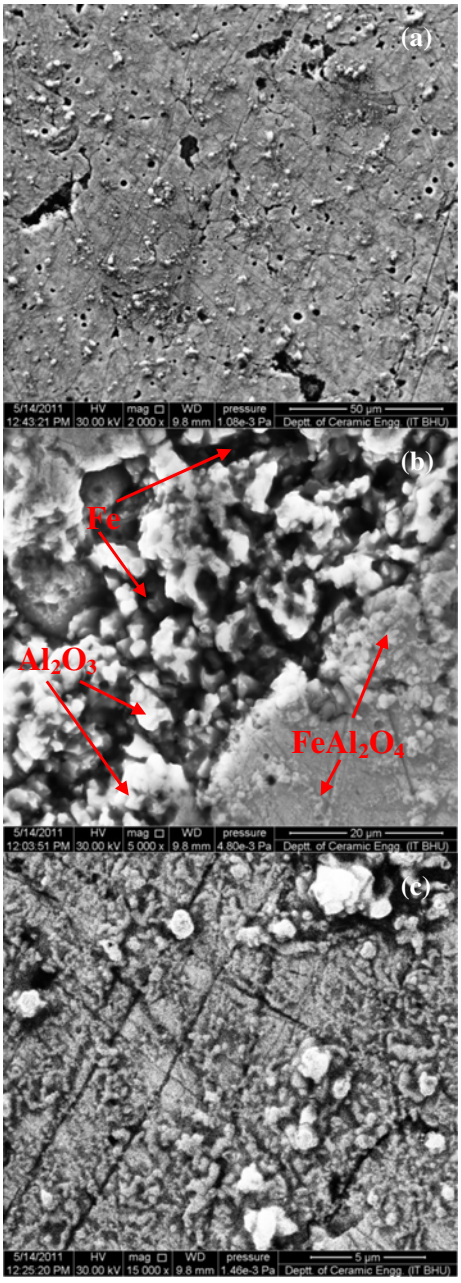

Figure 8. SEM micrographs of 5AFe1100(1): (**a**) 2000X, (**b**) 5000X and (**c**) 15000X magnifications.

The micrograph at 2000X magnification reveals the formation of highly dense Fe–Al_2O_3 metal matrix composite. The densified phase has got negligible amount of porosity. Figure 8(b) shows high magnification micrograph (5000X) of same sample. The larger black grains are of iron, white are of alumina whereas rest of the grayish grains are of iron aluminate which are formed as a result of reactive sintering. The same micrograph when viewed at 15000X (figure 8c) shows Al_2O_3 particles which are of sub-micrometer size. $FeAl_2O_4$ particles are of nanometer size which are formed during reaction sintering. The microstructure is similar to the microstructure of specimen 5AFe900(3) indicating that microstructure evolution changes similarly during reactive sintering by change of temperature or time of sintering.

3.3 *Density*

The density vs sintering temperature plots at different sintering times for 5% Al_2O_3 specimens are shown in figure 9. When sintering is carried out at 900 °C for 1 h, the sample 5AFe900(1) has lower value of density (4·33 g/cc). When sintering time is increased to 2 h, the value of density increases rapidly; thereafter, it remains constant with increasing the time to 3 h. Specimens sintered at 1000 and 1100 °C

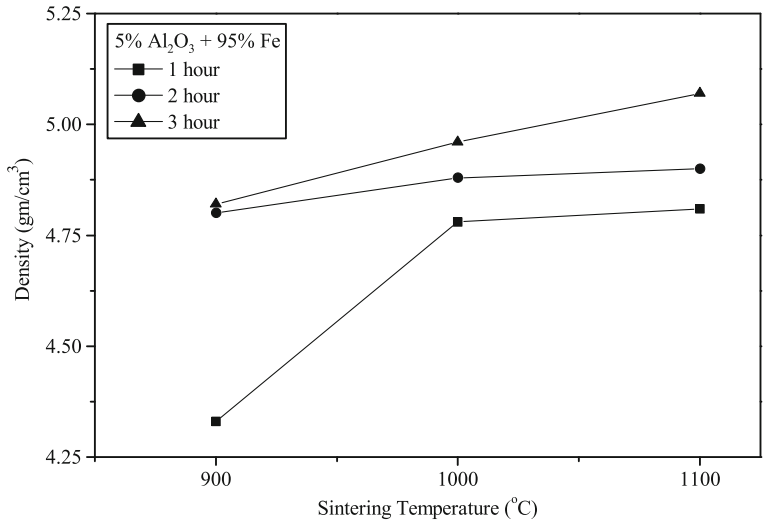

Figure 9. Density vs sintering temperature at different sintering times.

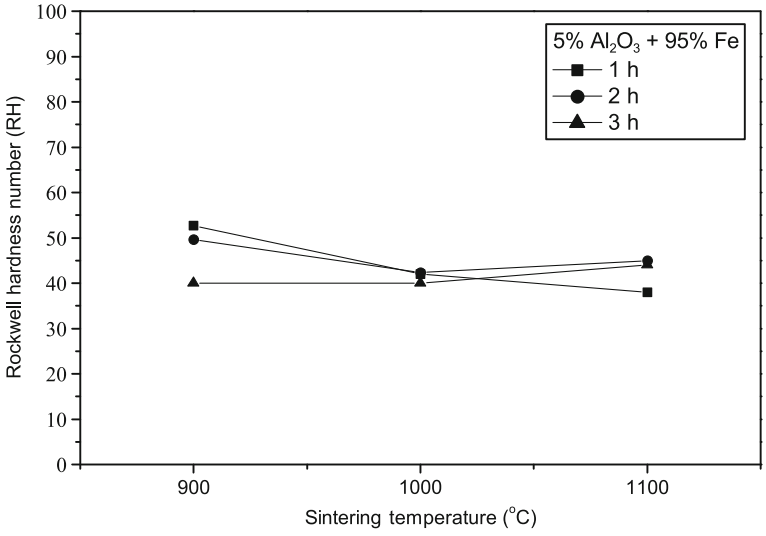

Figure 10. Hardness vs sintering temperature at different sintering times.

for 1, 2 and 3 h, density increases with sintering time in a regular fashion. More reaction takes place between iron and alumina with increasing sintering temperature and time. Highest densification is observed for specimen 5AFe1100(3), which is sintered at 1100 °C for 3 h (5·07 g/cc), the net densification is around 99%. The density increases with increasing sintering temperature and time (Karak *et al* 2011). Increase in density due to increase in chemical reaction (reactive sintering) cannot be answered definitely. It will depend on the difference of densities of reacting phases and the product phase.

3.4 *Hardness*

The hardness number was indicated by the instrument by initially applying a minor load of 10 kg and thereafter, applying a major load of 60 kg. Average hardness vs sintering temperature plots for different sintering times of 5% Al_2O_3 are shown in figure 10.

For specimen sintered at 900 °C, the hardness number decreases with increasing sintering time. There is a small decrease in hardness number for specimens sintered at 1000 °C with increasing sintering time. Hardness number for specimens sintered at 1100 °C initially increases with sintering time from 1 to 2 h and then decreases. Hardness number of specimens decreases with increasing sintering temperature up to 1000 °C; thereafter, it increases with temperature except for 1 h sintered specimen 5AFe1100(1). Hardness number of specimen 5AFe900(3) is same as that of specimen 5AFe1100(1).

The variation in hardness number of the specimens with sintering temperature and time can be explained on the basis

of nature of sintering in the composite for respective sintering times. Two types of sintering is proposed: (i) solid state sintering between Fe particles and (ii) reactive sintering between Fe and Al_2O_3 particles associated with the formation of iron aluminate. With first kind of sintering, there shall be no change in the fraction of ceramic reinforcement in the composite and metallic characteristics are enhanced due to densification resulting in the decrease in hardness number. With second kind of reactive sintering, content of aluminate phase, i.e. ceramic, increases resulting in an increase in hardness number. For lower sintering temperature, reactive sintering rate is smaller than that of solid state sintering amongst Fe particles and hardness number decreases with increasing sintering time. With increasing sintering temperature, reactive sintering rate increases leading to the formation of ceramic $FeAl_2O_4$ nanoparticles resulting in an increase in hardness number of the specimen with increasing sintering temperature. For 5% Al_2O_3 composition, when reactive sintering is complete, the hardness decreases with increasing sintering time from specimens 5AFe1100(2) to 5AFe1100(3). It is also found that nano-size iron aluminate ($FeAl_2O_4$) phase forms in between iron grains and bonds and interlocks those grains effectively.

3.5 *Compressive strength*

Prior to the compression test, the cross-sectional area and height of the samples were measured. Initially, the compression test was done on the specimen 5AFe900(2) under a load of 1500 kg, at which it was unable to bear the load. Compression tests on other specimens were, therefore, carried up to the safe limit of 1200 kg load. The load was applied on the samples gradually with a crosshead speed of 0·05 cm/min. Load vs deformation was recorded with the help of a chart recorder.

Stress vs strain plots for specimens 5AFe900(1), 5AFe1000(1) and 5AFe1100(1) sintered for 1 h are shown in figure 11(a–c). Initially, stress vs strain curve plot for all the three specimens is a straight line up to a particular stress (yield strength) beyond which specimen deforms

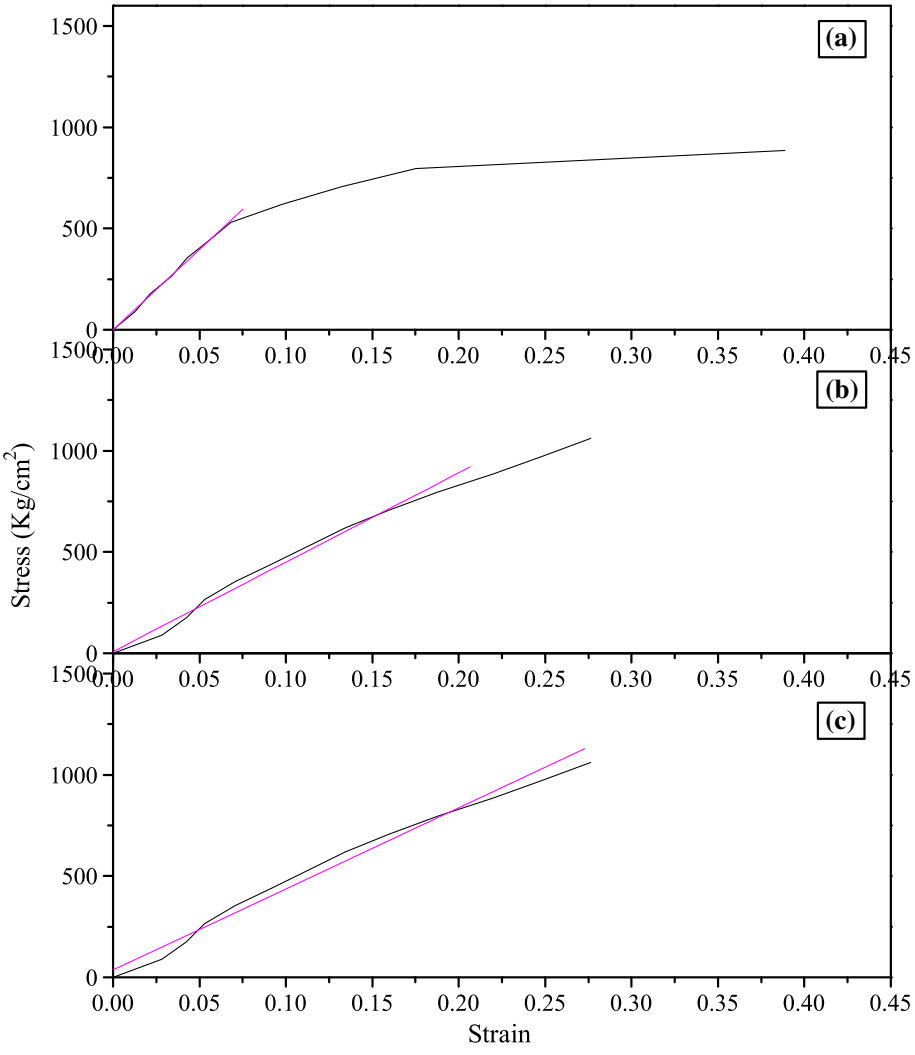

Figure 11. Stress vs strain plot for specimens: (**a**) 5AFe900(1), (**b**) 5AFe1000(1) and (**c**) 5AFe1100(1), sintered for 1 h.

without change in stress. Further compression of specimen leads to further increase in stress before failure. Compression modulus for different specimens was determined by fitting the initial part of the curve with straight line. Compression modulus and yield strength values for different samples sintered for 1 and 2 h are shown in table 1. The compressive modulus and yield strength of different specimens is in the range of 4000–8000 kg/cm^2 and 530–980 kg/cm^2, respectively. Compression modulus value decreases with increase in the sintering temperature while yield strength value of the specimen increases with an increase in the sintering temperature.

Table 1. Compression modulus and yield strength values of 5% for samples sintered for 1 and 2 h.

Sl. no.	Sample code	Compression modulus (kg/cm^2)	Yield strength (kg/cm^2)
1	5AFe900(1)	7924	530
2	5AFe1000(1)	4410	796
3	5AFe1100(1)	4005	973
4	5AFe900(2)	5073	530
5	5AFe1000(2)	3800	530
6	5AFe1100(2)	6739	442

The compressive stress–strain plots for specimens 5AFe900(2), 5AFe1000(2) and 5AFe1100(2) sintered at different temperatures for 2 h are shown in figure 12(a–c), respectively. Initially, stress vs strain curve is a straight line up to a particular stress (yield strength), beyond which specimen deforms without change in the stress. Further compression of specimen leads to further increase in stress before failure. Compression modulus for different specimens was determined by fitting the initial part of the curve with a straight line.

The compressive modulus and yield strength of different specimens is in the range of 3800–6800 kg/cm^2 and 440–530 kg/cm^2, respectively. Compression modulus initially decreases with increasing sintering temperature up to 1000 °C and increase thereafter.

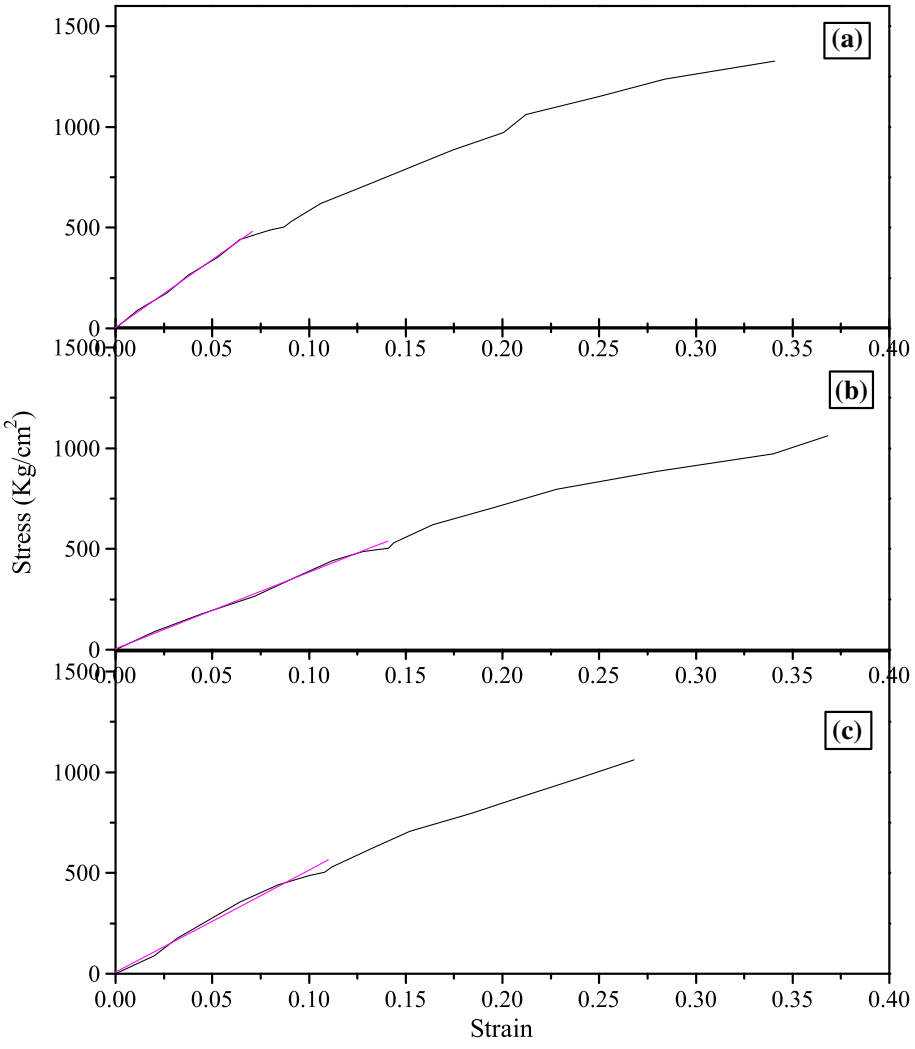

Figure 12. Stress vs strain plot for specimens: (**a**) 5AFe900(2), (**b**) 5AFe1000(2) and (**c**) 5AFe1100(2), sintered for 2 h.

The value of yield strength for specimens 5AFe900(2) and 5AFe1000(2) is more than that for 5AFe1100(2). The variation of compression modulus and yield strength can similarly be explained as hardness. Sintering leads to more ductility and reduces compression modulus, whereas formation of ceramic $FeAl_2O_4$ phase will increase compression modulus. The dip shown in figure 12 indicates the formation of initial crack and its propagation. Further, crack propagation is limited by the ceramic reinforcement which leads to increased toughness.

The overall phenomenon of compressive strength can be very well understood with the help of toughening mechanism in which the crack propagates, when the stress is exhibited by the composite specimen. Initially, when the stress increases, a slower cracking is being exhibited by surface of the specimen. Up to a certain stage, there is only bulging effect, whereas further increase of load breaks the sample from the surface, thus leading to an increase in the fracture toughness property.

4. Conclusions

(I) XRD plot shows formation of iron aluminate ($FeAl_2O_4$). This occurs because of reactive sintering process between iron and alumina.
(II) SEM micrograph shows formation of highly densified metal matrix composites with nanosize particles of iron aluminate.
(III) Densification increases with increase in the values of sintering temperature as well as time of sintering.
(IV) Variation in the hardness number depends upon the iron aluminate phase formation in the composite system and variation in iron aluminate phase depends upon sintering temperature and time, respectively.

Acknowledgements

The authors are thankful to Prof. G V S Sastry and late Prof. N Prasad, Department of Metallurgical Engineering, Indian Institute of Technology (Banaras Hindu University), Varanasi, for their valuable support.

References

Aldas K and Mat D M 2005 *J. Mater. Proc. Technol.* **160** 289
Chen S H and Wang T C 2002 *Acta Mechan.* **157** 113
Chua B W, Lu L and Lai M O 1999 *Compos. Struct.* **47** 595
Fedorchenko I M and Ivanova I I 1969 *Porosh. Metall.* **84** 23
Fligier A Wlodarczyk, Dobrzanski L A, Kremzer M and Adamiak M 2008 *J. Achiev. Mater. Manuf. Engg.* **27** 99
Karak S K, Chudobab T, Witczak Z, Lojkowski W and Manna I 2011 *Mater. Sci. Engg.* **A528** 7475
Karak S K, Majumdar J Dutta, Lojkowski W, Michalski A, Ciupinski L, Kurzydłowski K J and Manna I 2012 *Philos. Mag.* **92** 516
Konopka K and Ozieblo A 2001 *Mater. Char.* **46** 125
Miracle D B 2005 *Compos. Sci. Technol.* **65** 2526
Pagounis E, Talvitieb M and Lindroos V K 1996 *Compos. Sci. Technol.* **56** 1329
Rabiei A, Vendra L and Kishi T 2008 *Compos. Part A: Appl. Sci. Manuf.* **39** 294
Mehdi Rahimian, Naser Ehsani, Nader Parvin and Reza Baharvandi Hamid 2009 *J. Mater. Proc. Technol.* **209** 5387
Reddy B S B, Rajasekhar K, Venu M, Dilip J J S, Das Siddhartha and Das Karabi 2008 *J. Alloys Compd.* **465** 97
Rosso M 2006 *J. Mater. Proc. Technol.* **175** 364
Roy D, Ghosh S, Basumallick A and Basu B 2006 *Mater. Sci. Engg.* **A415** 202
Shen Y L and Chawla N 2001 *Mater. Sci. Engg.* **A297** 44
Tjong S C and Ma Z Y 2000 *Mater. Sci. Engg.* **29** 49
Torralba J M, Costa C E Da and Velasco F 2003 *J. Mater. Proc. Technol.* **133** 203
Wei Yueguang 2001 *Acta Mechan. Sinica* **17** ISSN 0567-7718